Stanford Exploration Project, Report 124, April 4, 2006, pages 17–33

Residual moveout in anisotropic angle-domain common image gathers with dipping reflectors

Pierre Jousselin and Biondo Biondi

ABSTRACT

We generalise to dipping reflectors the fundamental concepts for quantitatively relating perturbations in anisotropic parameters to the corresponding reflector movements in angle-domain common-image gathers (ADCIGs).
We apply the general methodology to the particular case of residual moveout (RMO) analysis of reflections from dipping reflectors in a vertical transverse isotropic (VTI) medium. Synthetic examples show the accuracy of the RMO curves predicted by our kinematic analysis.

INTRODUCTION

The fundamental concepts presented in Biondi (2005a) of quantitatively relating perturbations in anisotropic parameters to the corresponding reflector movements in angle-domain common-image gathers (ADCIGs) have been applied to flat reflectors. It showed on real data how measuring the residual moveout (RMO) in ADCIGs provides the quantitative information necessary to update the velocity function in a migration velocity analysis (MVA) procedure.

Aiming to generalize that methodology to the most general case, we derive an analytical analysis of residual moveout in anisotropic ADCIGs with dipping reflectors.

After deriving the kinematic analysis in the general case, we apply the general methodology to the particular case of residual moveout analysis of reflections from dipping reflectors in a vertical transverse isotropic (VTI) medium. Synthetic examples demonstrate the accuracy of the RMO curves predicted by our kinematic analysis. Furthermore, given the inaccuracy of the RMO curves predicted when assuming that the reflectors are flat, synthetic examples also demonstrate the usefulness of the generalization we present.

ANGLE-DOMAIN COMMON-IMAGE GATHERS

We first present a review of the theory for ADCIGs in anisotropic media from both a Kirchhoff and a "plane-wave" viewpoint (Biondi, 2005a). Those two are independent but yield the same result and therefore validate each other. We introduce the formulas we will use in the next sections.

Generalized migration impulse response in parametric form

The kinematic approach of anisotropic migration (Biondi, 2005a) is based on the generalization of integral migration to the computation of a prestack image that includes the subsurface offset dimension.

Theory of ADCIGs in anisotropic media from a Kirchhoff viewpoint

Figure 1 illustrates the generalization of the migration operator from a Kirchhoff viewpoint. Simple geometric relations allow us to derive the kinematics of the generalized migration operator. If we migrate an impulse recorded at time t_D, midpoint m_D and surface offset h_D, the migration impulse response can be expressed as follows:

$$z_\xi = L(\alpha_x,\gamma)\frac{\cos^2\alpha_x - \sin^2\gamma}{\cos\alpha_x\cos\gamma}, \tag{1}$$

$$m_\xi = m_D - L(\alpha_x,\gamma)\frac{\sin\alpha_x}{\cos\gamma}, \tag{2}$$

$$h_\xi = h_D - H = h_D - L(\alpha_x,\gamma)\frac{\sin\gamma}{\cos\alpha_x}, \tag{3}$$

where α_x is the group dip angle, γ is the group average aperture angle, z_ξ, m_ξ and h_ξ are the depth, midpoint and subsurface offset of the imaging point as illustrated in Figure 1. $L(\alpha_x,\gamma)$ is the average half-path length and is given by

$$L(\alpha_x,\gamma) = \frac{L_s+L_r}{2} = \frac{t_D}{(S_r+S_s)+(S_r-S_s)\tan\alpha_x\tan\gamma}, \tag{4}$$

where S_s and S_r are the group slowness along the source and receiver rays, respectively.

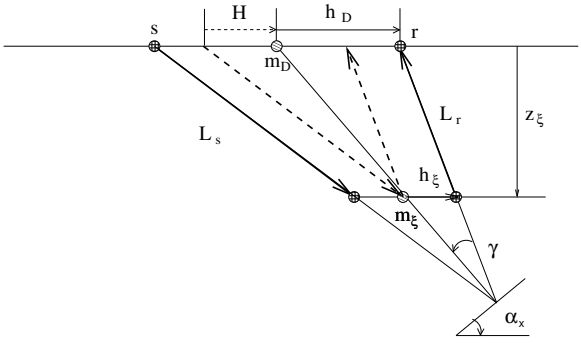

Figure 1: Geometry used for evaluating the impulse response of integral migration, generalized to produce a prestack image function of the subsurface offset h_ξ. pierre1-imp-resp [NR]

The expression for the generalized impulse response of prestack anisotropic migration leads to the analytical evaluation of the offset dip ($\frac{\partial z_\xi}{\partial h_\xi}\Big|_{m_\xi=\overline{m}_\xi}$) and midpoint dip ($\frac{\partial z_\xi}{\partial m_\xi}\Big|_{h_\xi=\overline{h}_\xi}$) along the planes tangent to the impulse response. When we adopt the Kirchhoff viewpoint, the group aperture angles can then be related to the offset dips in the image, and the group dip angles can be similarly related to the midpoint dips in the image.

Theory of ADCIGs in anisotropic media from a "plane-wave" viewpoint

From the "plane-wave" viewpoint of the theory of ADCIGs in anisotropic media, the expression for the generalized impulse response of prestack anisotriopic migration leads to the following expressions for the offset and midpoint dips:

$$\left.\frac{\partial z_\xi}{\partial h_\xi}\right|_{m_\xi=\overline{m}_\xi} = \frac{\tan\widetilde{\gamma}+\frac{\widetilde{S}_r-\widetilde{S}_s}{\widetilde{S}_r+\widetilde{S}_s}\tan\widetilde{\alpha}_x}{1-\frac{\widetilde{S}_r-\widetilde{S}_s}{\widetilde{S}_r+\widetilde{S}_s}\tan\widetilde{\alpha}_x\tan\widetilde{\gamma}} = \tan\widehat{\gamma}, \tag{5}$$

$$\left.\frac{\partial z_\xi}{\partial m_\xi}\right|_{h_\xi=\overline{h}_\xi} = \frac{\tan\widetilde{\alpha}_x+\frac{\widetilde{S}_r-\widetilde{S}_s}{\widetilde{S}_r+\widetilde{S}_s}\tan\widetilde{\gamma}}{1-\frac{\widetilde{S}_r-\widetilde{S}_s}{\widetilde{S}_r+\widetilde{S}_s}\tan\widetilde{\gamma}\tan\widetilde{\alpha}_x} = \tan\widehat{\alpha_x}, \tag{6}$$

where $\widetilde{\alpha_x}$ is the group dip angle, $\widetilde{\gamma}$ is the group average aperture angle, $\widehat{\alpha_x}$ and $\widehat{\gamma}$ are two angles we introduce and that are related to the midpoint and offset dips. $\widetilde{S}_s$ and $\widetilde{S}_r$ are the phase slownesses for the source and receiver wavefields, respectively. The phase aperture and group dip angles can then be related to the offset and midpoint image dips:

$$\tan\widetilde{\gamma} = \frac{\tan\widehat{\gamma}-\Delta_{\widetilde{S}}\tan\widetilde{\alpha}_x}{1+\Delta_{\widetilde{S}}\tan\widetilde{\alpha}_x\tan\widehat{\gamma}}, \tag{7}$$

$$\tan\widetilde{\alpha}_x = \frac{\tan\widehat{\alpha_x}-\Delta_{\widetilde{S}}\tan\widetilde{\gamma}}{1+\Delta_{\widetilde{S}}\tan\widetilde{\gamma}\tan\widehat{\alpha_x}}, \tag{8}$$

where $\Delta_{\widetilde{S}}$ is the "normalized slowness difference" $(\widetilde{S}_r-\widetilde{S}_s)/(\widetilde{S}_r+\widetilde{S}_s)$.

KINEMATICS OF THE ANGLE-DOMAIN TRANSFORMATION

In 2-D, ADCIGs are computed by applying a slant-stack decomposition to the prestack image along the subsurface-offset axis at a constant midpoint. The kinematics of the transformation are defined by the following change of variable:

$$\widehat{\gamma} = \arctan\left.\frac{\partial z_\xi}{\partial h_\xi}\right|_{m_\xi=\overline{m}_\xi}, \tag{9}$$

$$z_{\tilde{\gamma}} = z_\xi - h_\xi\tan\widehat{\gamma}, \tag{10}$$

where $z_{\tilde{\gamma}}$ is the depth of the image point after the transformation.

Geometric interpretation

Figure 2 provides a geometric interpretation of the transformation of an image point in the subsurface offset domain (z_ξ, h_ξ) to the corresponding image point in the angle-domain $(z_{\tilde{\gamma}}, \widetilde{\gamma})$. In this figure,

$$\beta_s = \alpha_x + \gamma, \tag{11}$$
$$\beta_r = \alpha_x - \gamma, \tag{12}$$
$$\widetilde{\beta}_s = \widetilde{\alpha}_x + \tilde{\gamma}, \tag{13}$$
$$\widetilde{\beta}_r = \widetilde{\alpha}_x - \tilde{\gamma}. \tag{14}$$

From a "plane-wave" viewpoint, the image point in the angle-domain is determined by the intersection of the lines passing through the points $(z_\xi, m_\xi \pm h_\xi)$ and tilted by $\widetilde{\beta}_s$ and $-\widetilde{\beta}_r$. This interpretation is consistent with the one for flat reflectors illustrated in Figure 3.

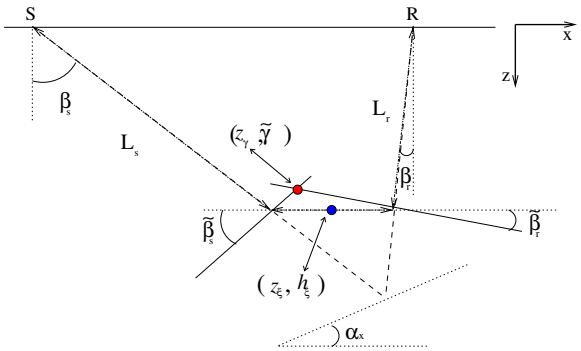

Figure 2: Geometry of the transformation to the angle-domain with a dipping reflector. The image point in the subsurface-offset domain (z_ξ, h_ξ) moves to the image point in the angle-domain $(z_{\tilde{\gamma}}, \widetilde{\gamma})$. pierre1-cig-2d-aniso-dipping-1 [NR]

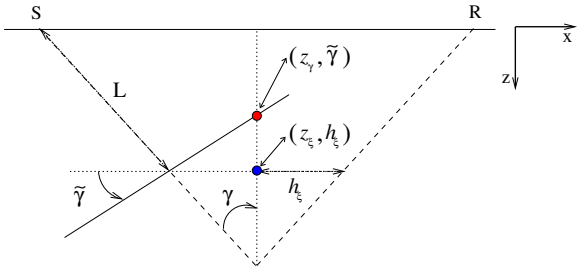

Figure 3: Geometry of the transformation to the angle-domain with a flat reflector. The image point in the subsurface-offset domain (z_ξ, h_ξ) moves to the image point in the angle-domain $(z_{\tilde{\gamma}}, \widetilde{\gamma})$. pierre1-cig-2d-aniso-flat-v1 [NR]

The geometric interpretation of the angle $\widehat{\gamma}$ is illustrated in Figure 4. According to equation (10), the depth of the image point in the angle-domain $z_{\tilde{\gamma}}$ is given by the intersection of the two lines passing through the points $(z_\xi, m_\xi \pm h_\xi)$ and tilted by $\pm\widehat{\gamma}$. For flat reflectors, $\widehat{\gamma} = \tilde{\gamma}$ (Biondi, 2005a), which is consistent with Figure 3.

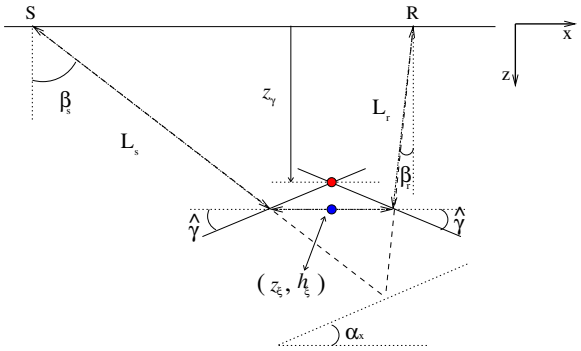

Figure 4: Geometric interpretation of the angle $\widehat{\gamma}$. pierre1-cig-2d-aniso-dipping-2 [NR]

Relationships between $\widehat{\gamma}$, $\tilde{\gamma}$ and γ

The angle $\tilde{\gamma}$ can be calculated from $\widehat{\gamma} = \arctan \frac{\partial z_\xi}{\partial h_\xi}\Big|_{m_\xi = \overline{m}_\xi}$ and $\widehat{\alpha_x} = \arctan \frac{\partial z_\xi}{\partial m_\xi}\Big|_{h_\xi = \overline{h}_\xi}$ by solving the two quadratic equations given by equations (7) and (8):

$$\left[\Delta\tilde{s}\tan\widehat{\alpha_x} - \left(\Delta\tilde{s}\right)^2\tan\widehat{\gamma}\right]\tan^2\tilde{\gamma} + \left[1 - \left(\Delta\tilde{s}\right)^2\right]\tan\tilde{\gamma} + \Delta\tilde{s}\tan\widehat{\alpha_x} - \tan\widehat{\gamma} = 0, \quad (15)$$

$$\left[\Delta\tilde{s}\tan\widehat{\gamma} - \left(\Delta\tilde{s}\right)^2\tan\widehat{\alpha_x}\right]\tan^2\tilde{\alpha}_x + \left[1 - \left(\Delta\tilde{s}\right)^2\right]\tan\tilde{\alpha}_x + \Delta\tilde{s}\tan\widehat{\gamma} - \tan\widehat{\alpha_x} = 0. \quad (16)$$

The angle γ can be estimated from $\tilde{\gamma}$ using

$$\tan\gamma = \frac{\tan\tilde{\gamma} + \frac{1}{\widetilde{V}}\frac{d\widetilde{V}}{d\tilde{\gamma}}}{1 - \frac{1}{\widetilde{V}}\frac{d\widetilde{V}}{d\tilde{\gamma}}\tan\tilde{\gamma}}. \quad (17)$$

RMO in ADCIGs

When the migration velocity is correct and the image is focused at zero subsurface offset, the transformation to angle domain does not change the depth of the image point, and the reflections are imaged at the same depth for all aperture angles. In contrast, when the reflections are not focused at zero offset, the transformation to the angle-domain maps the events at different depths for each different angle. The variability of the depth $z_{\tilde{\gamma}}$ with the aperture angle is described by the RMO function, which we want to measure and quantify as a function of the perturbation in anisotropic parameters encountered along the propagation paths.

ANISOTROPIC RESIDUAL MOVEOUT FOR DIPPING REFLECTORS

Having generalized to dipping angles the analysis of the kinematics of the offset-to-angle transformation, we generalize to dipping reflectors the analysis of the residual moveout in ADCIGs caused by errors in anisotropic velocity parameters. As in Biondi (2005a), we derive the RMO function by linearizing the relationship of the imaging depth in the angle domain with respect to perturbations in the anisotropic parameters. The linearization is evaluated

around the correct migration velocity function; that is, when the image in the subsurface-offset domain is well focused at zero offset. We derive relationships under the assumption that the velocity perturbations are limited to a homogeneous half-space above the reflector.

We use a notation that is the same as in Biondi (2005a): the VTI velocity function is described by the vector $\mathbf{V} = (V_V, V_H, V_N)$, where V_V is the velocity of a vertical ray, V_H is the velocity of a horizontal ray and V_N is the NMO velocity. The perturbations are defined as the combination of one multiplicative factor for each of the velocities (ρ_V) and one multiplicative factor for all velocities (ρ_{V_V},ρ_{V_H} and ρ_{V_N}): the perturbed velocity ${}_\rho\mathbf{V}$ is defined as:

$$ {}_\rho\mathbf{V} = \left({}_\rho V_V, {}_\rho V_H, {}_\rho V_N\right) = \rho_V \left(\rho_{V_V} V_V, \rho_{V_H} V_H, \rho_{V_N} V_N\right). \tag{18}$$

The velocity-parameter perturbation is a four-component vector $\boldsymbol{\rho}= \left(\rho_V, \rho_{V_V}, \rho_{V_H}, \rho_{V_N}\right)$.

In the case of dipping reflectors, the equation for the differentiation of the image point depth in the angle domain $z_{\tilde{\gamma}}$ with respect to the i-th component in the perturbation vector can be written:

$$ \frac{\partial z_{\tilde{\gamma}}}{\partial \rho_i} = \frac{\partial z_{\tilde{\gamma}}}{\partial L}\frac{\partial L}{\partial \rho_i} + \frac{\partial z_{\tilde{\gamma}}}{\partial \beta_s}\frac{\partial \beta_s}{\partial \rho_i} + \frac{\partial z_{\tilde{\gamma}}}{\partial \beta_r}\frac{\partial \beta_r}{\partial \rho_i} + \frac{\partial z_{\tilde{\gamma}}}{\partial \tilde{\beta}_s}\frac{\partial \tilde{\beta}_s}{\partial \rho_i} + \frac{\partial z_{\tilde{\gamma}}}{\partial \tilde{\beta}_r}\frac{\partial \tilde{\beta}_r}{\partial \rho_i}. \tag{19}$$

Expanding the term $\frac{\partial L}{\partial \rho_i}$ of equation (19), we get

$$ \begin{aligned} \frac{\partial L}{\partial \rho_i} &= \frac{1}{2}\left(\frac{\partial L_s}{\partial \rho_i} + \frac{\partial L_r}{\partial \rho_i}\right) \\ &= \frac{1}{2}\left(\frac{\partial L_s}{\partial S_s}\left(\frac{\partial S_s}{\partial \rho_i} + \frac{\partial S_s}{\partial \beta_s}\right) + \frac{\partial L_r}{\partial S_r}\left(\frac{\partial S_r}{\partial \rho_i} + \frac{\partial S_r}{\partial \beta_r}\right)\right). \end{aligned} \tag{20}$$

Equation (19) can then be written

$$ \begin{aligned} \frac{\partial z_{\tilde{\gamma}}}{\partial \rho_i} &= \frac{1}{2}\frac{\partial z_{\tilde{\gamma}}}{\partial L}\left(\frac{\partial L_s}{\partial S_s}\frac{\partial S_s}{\partial \rho_i} + \frac{\partial L_r}{\partial S_r}\frac{\partial S_r}{\partial \rho_i}\right) \\ &+ \left(\frac{1}{2}\frac{\partial z_{\tilde{\gamma}}}{\partial L_s}\frac{\partial L_s}{\partial S_s}\frac{\partial S_s}{\partial \beta_s} + \frac{\partial z_{\tilde{\gamma}}}{\partial \beta_s}\right)\frac{\partial \beta_s}{\partial \rho_i} \\ &+ \left(\frac{1}{2}\frac{\partial z_{\tilde{\gamma}}}{\partial L_r}\frac{\partial L_r}{\partial S_r}\frac{\partial S_r}{\partial \beta_r} + \frac{\partial z_{\tilde{\gamma}}}{\partial \beta_r}\right)\frac{\partial \beta_r}{\partial \rho_i} \\ &+ \frac{\partial z_{\tilde{\gamma}}}{\partial \beta_s}\frac{\partial \beta_s}{\partial \rho_i} + \frac{\partial z_{\tilde{\gamma}}}{\partial \beta_r}\frac{\partial \beta_r}{\partial \rho_i}. \end{aligned} \tag{21}$$

Geometric interpretation of the movements of the image point in the angle-domain

The geometric interpretation of the angle-domain transformation kinematics allows us to simplify equation (21) by showing that the terms multiplying the partial derivatives with respect to the angles are zero. Equation (21) simplifies to

$$ \frac{\partial z_{\tilde{\gamma}}}{\partial \rho_i} = \frac{1}{2}\frac{\partial z_{\tilde{\gamma}}}{\partial L}\left(\frac{\partial L_s}{\partial S_s}\frac{\partial S_s}{\partial \rho_i} + \frac{\partial L_r}{\partial S_r}\frac{\partial S_r}{\partial \rho_i}\right). \tag{22}$$

Linearized perturbations caused by changes in L

Figure 5 graphically illustrates the image perturbation related to the first term in equation (22). It shows the movement of the image points (both in the subsurface-offset domain and the angle domain) caused by changes in the ray length L. **Linearized perturbations**

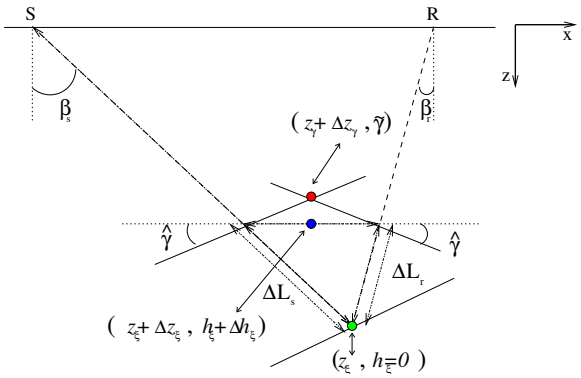

Figure 5: Linearized perturbations of the image-point locations caused by changes in the ray length L. pierre1-cig-2d-aniso-delta1-dipping-1 [NR]

caused by changes in β_s

Figure 6 graphically illustrates the image perturbation related to the second term in equation (22). Perturbations in the angle β_s cause the subsurface offset-domain image to move along the tangent to the incident wavefront. Since this movement is constraint along the tangent, the image point in the angle-domain does not move no matter how large the corresponding movement in the subsurface offset domain is. **Linearized perturbations caused**

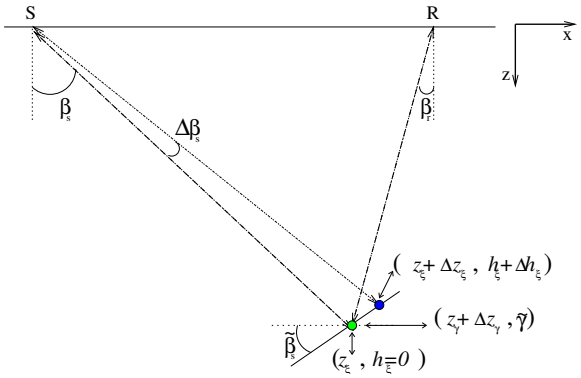

Figure 6: Linearized perturbations of the image-point locations caused by changes in β_s. pierre1-cig-2d-aniso-delta2-dipping-1 [NR]

by changes in $\tilde{\beta}_s$

Figure 7 graphically illustrates the image perturbation related to the third term in equation (22). Since we linearize the depth of the image point around the correct migration velocity function, perturbations in the angle $\tilde{\beta}_s$ don't affect the depth of the imaging point (it is the main concept of ADCIGs).

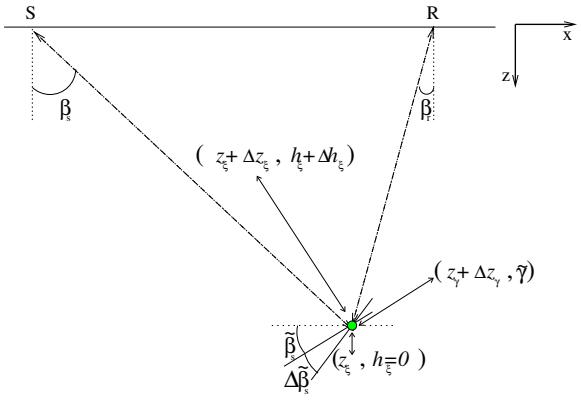

Figure 7: Linearized perturbations of the image-point locations caused by changes in $\tilde{\beta}_s$. pierre1-cig-2d-aniso-delta3-dipping-1 [NR]

Evaluation of the different terms in equation (22)

We show in Appendix A (equations (A-2) and (A-6))

$$\frac{\partial z_{\tilde{\gamma}}}{\partial L} = \frac{\cos^2\alpha_x - \sin^2\gamma}{\cos\alpha_x \cos\gamma} + \frac{\sin\gamma}{\cos\alpha_x}\tan\widehat{\gamma}, \tag{23}$$

and

$$\frac{\partial L_s}{\partial S_s} = -\frac{z_\xi}{S_s\cos(\beta_s)} = -\frac{z_\xi}{S_s\cos(\alpha_x+\gamma)}, \tag{24}$$

$$\frac{\partial L_r}{\partial S_r} = -\frac{z_\xi}{S_r\cos(\beta_r)} = -\frac{z_\xi}{S_r\cos(\alpha_x-\gamma)}. \tag{25}$$

Using equations (23), (24) and (25), the relationship of the imaging depth in the angle domain with respect to perturbations in the anisotropic parameters can eventually be written as follows:

$$\frac{\partial z_{\tilde{\gamma}}}{\partial \rho_i} = -\frac{z_\xi}{2}\left(\frac{\cos^2\alpha_x - \sin^2\gamma}{\cos\alpha_x\cos\gamma} + \frac{\sin\gamma}{\cos\alpha_x}\tan\widehat{\gamma}\right)\left(\frac{1/S_s}{\cos(\alpha_x+\gamma)}\frac{\partial S_s}{\partial\rho_i} + \frac{1/S_r}{\cos(\alpha_x-\gamma)}\frac{\partial S_r}{\partial\rho_i}\right). \tag{26}$$

This is the fundamental equation of this section, extending the equation given in Biondi (2005a) to include dipping reflectors.

The residual moveout Δz_{RMO} is defined as the difference between the reflector movement at finite aperture angle and the reflector movement at normal incidence. The latter is given by

$$\left.\frac{\partial z_{\tilde{\gamma}}}{\partial\rho_i}\right|_{\gamma=0} = -\frac{z_\xi}{S(\alpha_x)}\frac{\partial S(\alpha_x)}{\partial\rho_i}. \tag{27}$$

RMO function with uniform scaling of velocity

In case of uniform scaling of velocity, the derivative of the slowness with respect to a uniform scaling of the velocity has a simple form:

$$\frac{\partial S(x)}{\partial\rho_V} = -S(x). \tag{28}$$

The derivatives of the imaging depth $z_{\tilde{\gamma}}$ and of the residual moveout with respect to the perturbation component ρ_V have the following forms (refer to equations (A-14) and (A-16)):

$$\frac{\partial z_{\tilde{\gamma}}}{\partial \rho_i} = z_\xi \left(1 + \frac{1-\sin^2\gamma}{\cos^2\alpha_x - \sin^2\gamma} \tan\gamma \tan\widehat{\gamma} \right), \tag{29}$$

$$\frac{\partial \Delta z_{\text{RMO}}}{\partial \rho_V} = z_\xi \frac{1-\sin^2\gamma}{\cos^2\alpha_x - \sin^2\gamma} \tan\gamma \tan\widehat{\gamma}. \tag{30}$$

The dependence of equation (30) on the group angles increases the complexity of its use. However, we showed in the preceding section that it is possible to compute the angle γ from $\widehat{\gamma}$. We first compute $\tilde{\gamma}$ from $\widehat{\gamma}$ by solving a system of two quadratic equations (equations (15) and (16)) then computes γ from $\tilde{\gamma}$ by using equation (17). The computational cost of evaluating the group angles is negligible and it is important to introduce the distinction between the "three aperture angles": γ, $\tilde{\gamma}$ and $\widehat{\gamma}$.

Equations (30) and (29) are consistent with the ones derived in the isotropic case with dipping reflectors (Biondi and Symes, 2003). Under the assumption that the medium is isotropic, $\widehat{\gamma} = \gamma$ and the derivatives of the imaging depth $z_{\tilde{\gamma}}$ and of the residual moveout with respect to the perturbation component ρ_V are

$$\left.\frac{\partial z_{\tilde{\gamma}}}{\partial \rho_i}\right|_{\text{iso}} = z_\xi \left(1 + \frac{\sin^2\gamma}{\cos^2\alpha_x - \sin^2\gamma} \right), \tag{31}$$

$$\left.\frac{\partial \Delta z_{\text{RMO}}}{\partial \rho_V}\right|_{\text{iso}} = z_\xi \frac{\sin^2\gamma}{\cos^2\alpha_x - \sin^2\gamma}. \tag{32}$$

RMO function with arbitrary scaling of velocity

The derivatives of $z_{\tilde{\gamma}}$ and Δz_{RMO} with respect to arbitrary perturbations of the individual velocity components (i.e. V_V, V_H, and V_N) have no simple form in the case of dipping reflectors and depend on the particular form chosen to approximate the slowness function. The derivatives of $z_{\tilde{\gamma}}$ are

$$\frac{\partial z_\gamma}{\partial \rho_{V_V}} = -\frac{z_\xi}{2} \left(\frac{\cos^2\alpha_x - \sin^2\gamma}{\cos\alpha_x \cos\gamma} + \frac{\sin\gamma}{\cos\alpha_x} \tan\widehat{\gamma} \right) \left(\frac{1/S_s}{\cos(\alpha_x+\gamma)} \frac{\partial S_s}{\partial \rho_{V_V}} + \frac{1/S_r}{\cos(\alpha_x-\gamma)} \frac{\partial S_r}{\partial \rho_{V_V}} \right), \tag{33}$$

$$\frac{\partial z_\gamma}{\partial \rho_{V_H}} = -\frac{z_\xi}{2} \left(\frac{\cos^2\alpha_x - \sin^2\gamma}{\cos\alpha_x \cos\gamma} + \frac{\sin\gamma}{\cos\alpha_x} \tan\widehat{\gamma} \right) \left(\frac{1/S_s}{\cos(\alpha_x+\gamma)} \frac{\partial S_s}{\partial \rho_{V_H}} + \frac{1/S_r}{\cos(\alpha_x-\gamma)} \frac{\partial S_r}{\partial \rho_{V_H}} \right), \tag{34}$$

$$\frac{\partial z_\gamma}{\partial \rho_{V_N}} = -\frac{z_\xi}{2} \left(\frac{\cos^2\alpha_x - \sin^2\gamma}{\cos\alpha_x \cos\gamma} + \frac{\sin\gamma}{\cos\alpha_x} \tan\widehat{\gamma} \right) \left(\frac{1/S_s}{\cos(\alpha_x+\gamma)} \frac{\partial S_s}{\partial \rho_{V_N}} + \frac{1/S_r}{\cos(\alpha_x-\gamma)} \frac{\partial S_r}{\partial \rho_{V_N}} \right). \tag{35}$$

Conversion of depth errors into traveltime errors in heterogeneous media

The same relationships can be easily adapted to heterogeneous media (Biondi, 2005b) by converting the depth errors in ADCIGs into traveltime errors that can used for tomography.

The conversion to traveltime errors is done by rewriting the chain of partial derivatives:

$$\begin{aligned}\frac{\partial z_\gamma}{\partial t} &= \frac{\partial z_\gamma}{\partial L}\frac{\partial L}{\partial t},\\ \frac{\partial z_\gamma}{\partial t} &= \left(\frac{\cos^2\alpha_x-\sin^2\gamma}{\cos\alpha_x\cos\gamma}+\frac{\sin\gamma}{\cos\alpha_x}\tan\widehat{\gamma}\right)\frac{S_r+S_s}{1+\Delta_{\tilde{S}}\tan(\alpha_x)\tan\gamma}.\end{aligned} \tag{36}$$

Synthetic-data examples of RMO functions in ADCIGs

To verify the accuracy of the RMO functions derived in this section, we perform several numerical tests using synthetic data modeled and migrated using an anisotropic source-receiver modeling program and its adjoint. As in Biondi (2005b), this program performed depth extrapolation by numerically solving the following dispersion relation:

$$k_z = \frac{\omega}{V_V}\sqrt{\frac{\omega^2-{V_H}^2k_x^2}{\omega^2+\left({V_N}^2-{V_H}^2\right)k_x^2}}, \tag{37}$$

where ω is the temporal frequency, and k_x and k_z are the horizontal and vertical wavenumbers, respectively. This dispersion relation corresponds to the following slowness function (Fowler, 2003):

$$2S^2_{\rm VTI}(\theta) = S^2_{\rm Ell}(\theta)+\sqrt{S^4_{\rm Ell}(\theta)+{S_V}^2\left({S_N}^2-{S_H}^2\right)\sin^2 2\theta}, \tag{38}$$

where,

$$S^2_{\rm Ell}(\theta) = {S_V}^2\cos^2\theta+{S_H}^2\sin^2\theta, \tag{39}$$

is the elliptical component.

We tested the theory with the set of anisotropic Thomsen parameters of the Taylor Sand ($\epsilon = 0.110, \delta = -0.035 \rightarrow \eta = .155$) described in Tsvankin (2001). Figures 8 to 10 show examples of the application of the RMO function expressed in equation (30) when perturbing the velocity uniformly ($\rho_V = .95$). In the different examples, we didn't approximate the values of γ but computed them from the values of $\widehat{\gamma}$.

Figure 8 shows that for flat reflectors, the RMO function we derived accurately tracks the actual RMO function when the perturbations are sufficiently small to be within the range of accuracy of the linearization. This is consistent with the results presented in Biondi (2005b). The relative lack of accuracy at large aperture angle is due to the limited offset range we used for the modeling and the migration.

The top panel of Figure 9 shows that for a 15° dipping reflector the RMO function we derived accurately tracks the actual RMO function (the relative lack of accuracy at large aperture angle is due to the limited offset range we used). However the bottom panel shows that the use of the RMO function given in Biondi (2005b) (i.e. assuming that the reflector is flat) gives comparable results.

The top panel of Figure 9 shows that for a 30° dipping reflector, the RMO function we derived perfectly matches the actual RMO (we used a larger offset range). The bottom panel shows that the RMO function given in Biondi (2005b) (i.e. assuming that the reflector is flat) gives poor results. It justifies a posteriori the need for generalizing to dipping reflectors the concepts of quantitatively relating perturbations in anisotropic parameters to the corresponding reflector movements in anisotropic ADCIGs.

CONCLUSIONS

In this paper, we generalized to dipping reflectors the fundamental concepts for quantitatively relating perturbations in anisotropic parameters to the corresponding reflector movements in ADCIGs.

We applied that general methodology to the particular case of RMO analysis of reflections from dipping reflectors in a VTI medium. Our synthetic examples demonstrate the accuracy of the RMO curves predicted by our kinematic analysis and the inaccuracy of the RMO curves predicted when assuming that the reflectors are flat. It proves the usefulness of our generalization we presented in this paper. It should enable accurate migration velocity analysis procedures in complex areas where anisotropic wavefield continuation migration is required.

REFERENCES

Biondi, B. and W. W. Symes, 2003, Angle-domain common-image gathers for migration velocity analysis by wavefield-continuation imaging: Geophysics, **69**, 1283–1298.

Biondi, B., 2005a, Angle-domain common image gathers for anisotropic migration: SEP–**123**.

Biondi, B., 2005b, Residual moveout in anisotropic angle-domain common image gathers: SEP–**123**.

Fowler, P., 2003, Practical VTI approximations: a systematic anatomy: Journal of Applied Geophysics, **69**, 347–367.

Tsvankin, I., 2001, Seismic signatures and analysis of reflection data in anisotropic media: Elsevier Science.

APPENDIX A

DERIVATION OF THE DERIVATIVE OF THE ANGLE-DOMAIN DEPTH WITH RESPECT TO THE COMPONENTS OF THE PERTURBATION VECTOR

Derivation of equation (26)

- Using the kinematics of the transformation to the angle domain (equation (10)) and the equations of the migration impulse response (equations (1) and (3)),

$$\frac{\partial z_{\tilde{\gamma}}}{\partial L} = \frac{\partial z_\xi}{\partial L} - \frac{\partial h_\xi}{\partial L}\tan\widehat{\gamma}, \tag{A-1}$$

$$\frac{\partial z_{\tilde{\gamma}}}{\partial L} = \frac{\cos^2\alpha_x - \sin^2\gamma}{\cos\alpha_x\cos\gamma} + \frac{\sin\gamma}{\cos\alpha_x}\tan\widehat{\gamma}. \tag{A-2}$$

- Differentiating the equality $L_s S_s + L_r S_r = t_D$ with respect to S_s,

$$\frac{\partial L_s}{\partial S_s} S_s + L_s = 0, \tag{A-3}$$

$$\frac{\partial L_s}{\partial S_s} = -\frac{L_s}{S_s}. \tag{A-4}$$

Using the simple geometric relationship $L_s\cos\beta_s = z_\xi$, we eventually get

$$\frac{\partial L_s}{\partial S_s} = -\frac{z_\xi}{S_s\cos\beta_s} = -\frac{z_\xi}{S_s\cos(\alpha_x+\gamma)}. \tag{A-5}$$

From the geometric relationship $L_r\cos\beta_r = z_\xi$, we similarly show

$$\frac{\partial L_r}{\partial S_r} = -\frac{z_\xi}{S_r\cos\beta_r} = -\frac{z_\xi}{S_r\cos(\alpha_x-\gamma)}. \tag{A-6}$$

Derivation of equation (29)

In case of uniform scaling of velocity,

$$\frac{\partial z_{\tilde{\gamma}}}{\partial \rho_V} = -\frac{z_\xi}{2}\left(\frac{\cos^2\alpha_x - \sin^2\gamma}{\cos\alpha_x\cos\gamma} + \frac{\sin\gamma}{\cos\alpha_x}\tan\widehat{\gamma}\right)\left(\frac{1}{S_s\cos(\alpha_x+\gamma)}\frac{\partial S_s}{\partial \rho_i} + \frac{1}{S_r\cos(\alpha_x-\gamma)}\frac{\partial S_r}{\partial \rho_i}\right),$$

$$\frac{\partial z_{\tilde{\gamma}}}{\partial \rho_V} = -\frac{z_\xi}{2}\left(\frac{\cos^2\alpha_x - \sin^2\gamma}{\cos\alpha_x\cos\gamma} + \frac{\sin\gamma}{\cos\alpha_x}\tan\widehat{\gamma}\right)\left(-\frac{S_s}{S_s\cos(\alpha_x+\gamma)} - \frac{S_r}{S_r\cos(\alpha_x-\gamma)}\right),$$

$$\frac{\partial z_{\tilde{\gamma}}}{\partial \rho_V} = \frac{z_\xi}{2}\left(\frac{\cos^2\alpha_x - \sin^2\gamma}{\cos\alpha_x\cos\gamma} + \frac{\sin\gamma}{\cos\alpha_x}\tan\widehat{\gamma}\right)\left(\frac{1}{\cos(\alpha_x+\gamma)} + \frac{1}{\cos(\alpha_x-\gamma)}\right). \tag{A-7}$$

The quantity $\frac{1}{\cos(\alpha_x+\gamma)}+\frac{1}{\cos(\alpha_x-\gamma)}$ can be written

$$\begin{aligned}
\frac{1}{\cos(\alpha_x+\gamma)}+\frac{1}{\cos(\alpha_x-\gamma)} &= \frac{\cos(\alpha_x+\gamma)+\cos(\alpha_x-\gamma)}{\cos(\alpha_x+\gamma)\cos(\alpha_x-\gamma)}, && \text{(A-8)}\\
&= \frac{2\cos\alpha_x\cos\gamma}{\frac{\cos(2\alpha_x)+\cos(2\gamma)}{2}}, && \text{(A-9)}\\
&= \frac{2\cos\alpha_x\cos\gamma}{\frac{2\cos^2\alpha_x-1+2\cos^2\gamma-1}{2}}, && \text{(A-10)}\\
\frac{1}{\cos(\alpha_x+\gamma)}+\frac{1}{\cos(\alpha_x-\gamma)} &= \frac{2\cos\alpha_x\cos\gamma}{\cos^2\alpha_x-\sin^2\gamma}. && \text{(A-11)}
\end{aligned}$$

Using equation (A-11), equation (A-7) simplifies to

$$\begin{aligned}
\frac{\partial z_{\tilde{\gamma}}}{\partial \rho_V} &= z_\xi\left(1+\frac{\sin\gamma}{\cos\alpha_x}\frac{\cos\alpha_x\cos\gamma}{\cos^2\alpha_x-\sin^2\gamma}\tan\widehat{\gamma}\right), && \text{(A-12)}\\
&= z_\xi\left(1+\frac{\sin\gamma\cos\gamma}{\cos^2\alpha_x-\sin^2\gamma}\tan\widehat{\gamma}\right), && \text{(A-13)}\\
\frac{\partial z_{\tilde{\gamma}}}{\partial \rho_V} &= z_\xi\left(1+\frac{1-\sin^2\gamma}{\cos^2\alpha_x-\sin^2\gamma}\tan\gamma\tan\widehat{\gamma}\right). && \text{(A-14)}
\end{aligned}$$

Derivation of equation (30)

Recalling equation (27),

$$\left.\frac{\partial z_{\tilde{\gamma}}}{\partial \rho_i}\right|_{\gamma=0} = -\frac{z_\xi}{S(\alpha_x)}\frac{\partial S(\alpha_x)}{\partial \rho_i},$$

in case of uniform scaling of velocity,

$$\left.\frac{\partial z_{\tilde{\gamma}}}{\partial \rho_V}\right|_{\gamma=0} = z_\xi. \qquad \text{(A-15)}$$

The derivative of the residual moveout with respect to the perturbation component ρ_V has the following form:

$$\frac{\partial \Delta z_{\mathrm{RMO}}}{\partial \rho_V} = z_\xi\frac{1-\sin^2\gamma}{\cos^2\alpha_x-\sin^2\gamma}\tan\gamma\tan\widehat{\gamma}. \qquad \text{(A-16)}$$

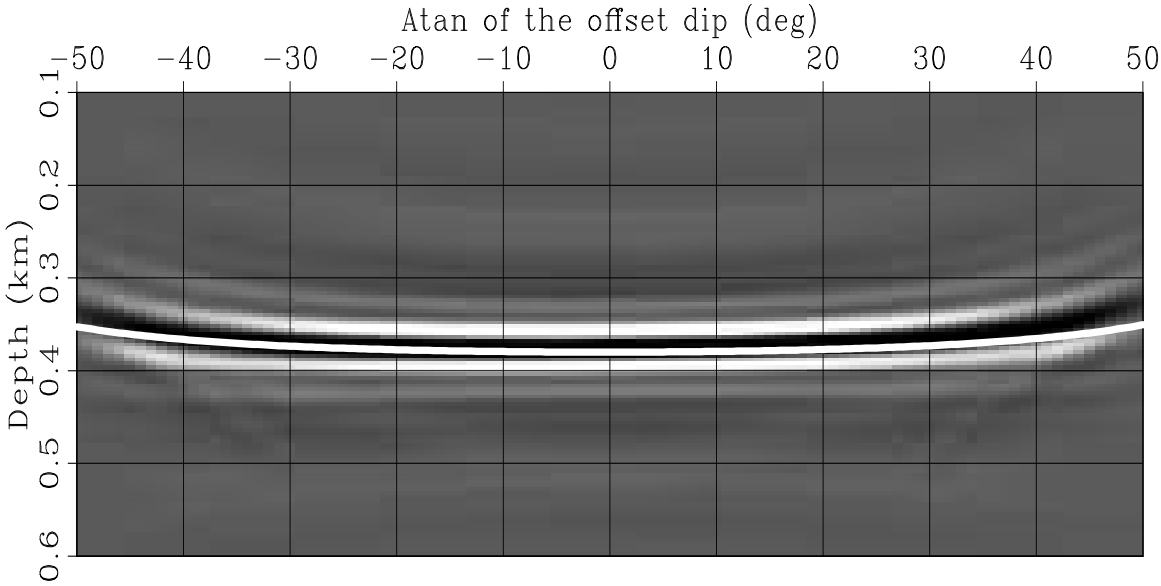

Figure 8: ADCIGs obtained for a flat reflector when a constant anisotropic velocity was perturbed by $\rho_V = .95$. Superimposed onto the images is the RMO function computed using the RMO function we derive in this paper (equation (30)). pierre1-Rho-95-Alpha-0 [CR]

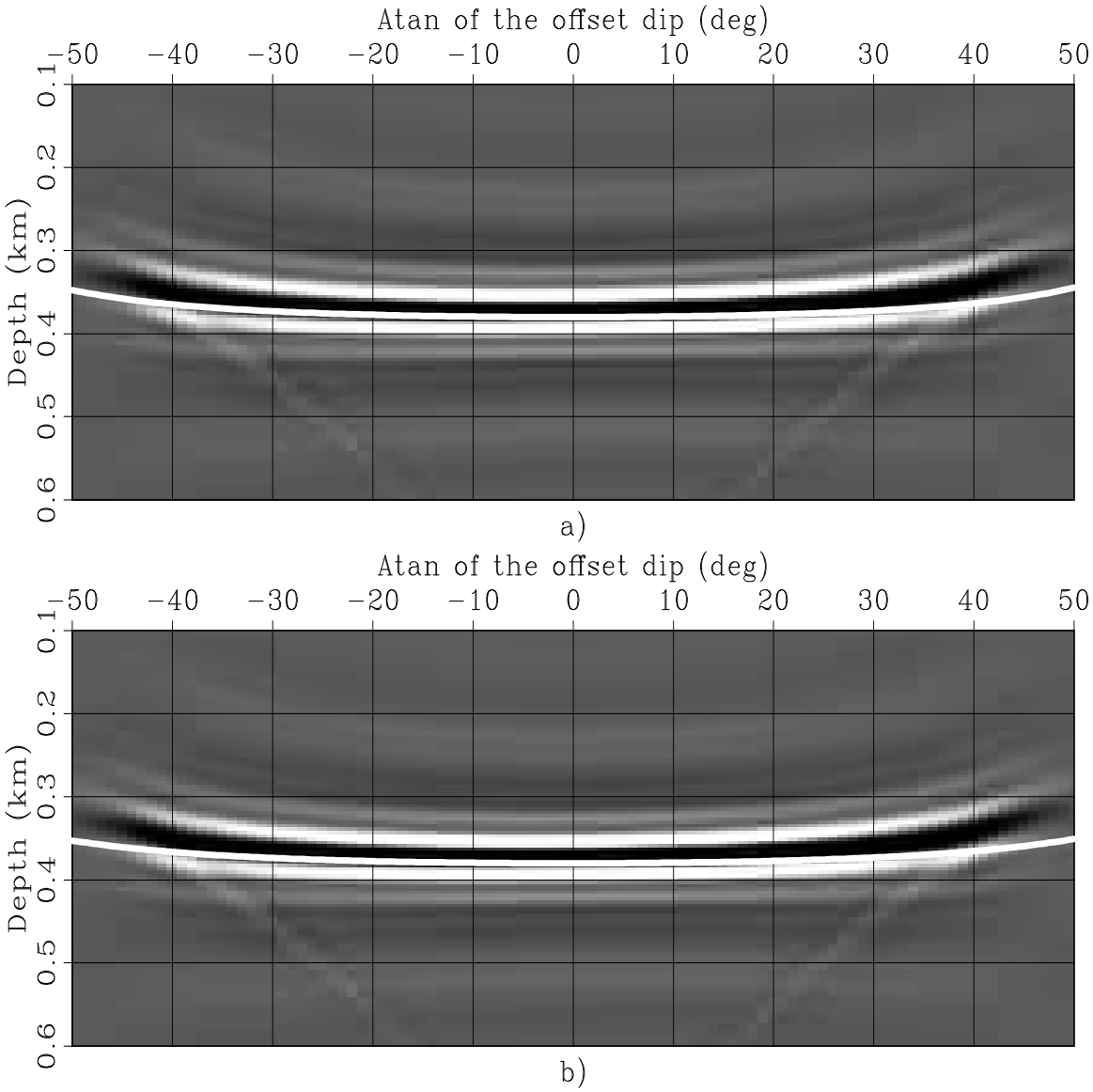

Figure 9: ADCIGs obtained for a 15° dipping reflector when a constant anisotropic velocity was perturbed by $\rho_V = .95$. Superimposed onto the images are the RMO functions computed: a) using the RMO function we derived in this paper (equation (30)); b) assuming that the reflector is flat, i.e. using the equation derived in Biondi (2005b). pierre1-Rho-95-Alpha-15 [CR]

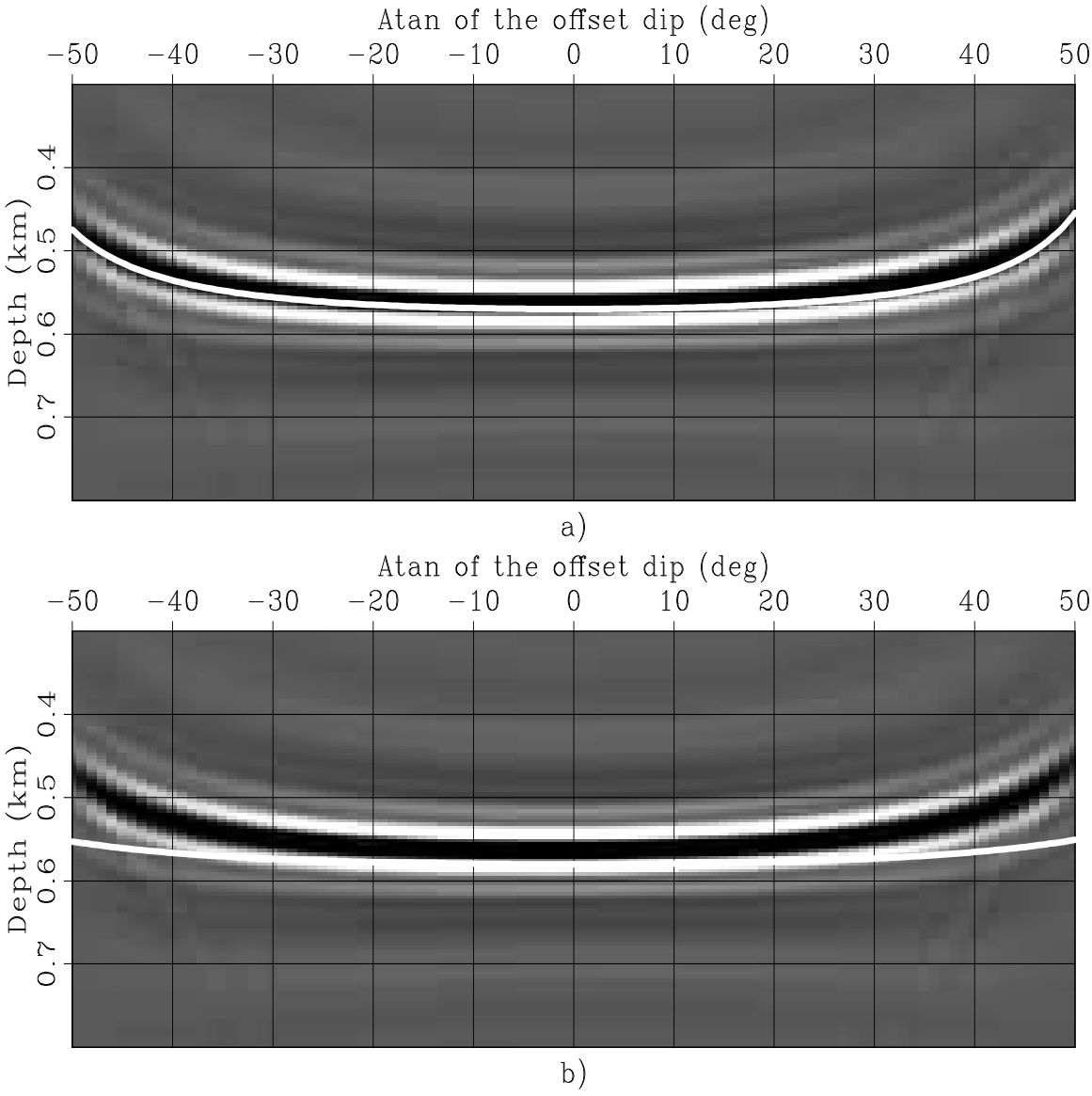

Figure 10: ADCIGs obtained for a 30° dipping reflector when a constant anisotropic velocity was perturbed by $\rho_V = .95$. Superimposed onto the images are the RMO functions computed: a) using the RMO function we derived in this paper (equation (30)); b) assuming that the reflector is flat, i.e. using the equation derived in Biondi (2005b) pierre1-Rho-95-Alpha-30 [CR]